SeDIF Conference

2nd International Conference on
Seismic Design of Industrial Facilities
Aachen, 04.-05.03.2020

Study of seismic effects in pipelines using Generalized Beam Theory

Abinet K. Habtemariam[1], **Volkmar Zabel** [2], **Carsten Könke** [3], **Marcelo J. Bianco**[4], **Fabiola Tartaglione**[5]

Institute of Structural Mechanics
Bauhaus-Universität Weimar, Marienstr. 15, 99421 Weimar, Germany
[1] abinet.habtemariam@uni-weimar.de
[2] volkmar.zabel@uni-weimar.de
[3] carsten.koenke@uni-weimar.de
[4] marcelo.jose.bianco@uni-weimar.de
[5] fabiola.tartaglione@uni-weimar.de

ABSTRACT

Pipelines in earthquake-prone regions can be susceptible to damage through different failure mechanisms. For above ground pipeline systems, investigating these failures requires a numerical method that appropriately describes the pipe, the support system, their interaction and failure modes characterised by local cross-sectional deformations. Common beam element models using springs for the supports have limitations with respect to failure description as they can usually not take into account the deformation of the cross-section. On the other hand, shell elements are capable of describing the respective failure mechanisms but require a higher degree of discretisation and result in models of high dimension which causes high computational costs.

In this paper, the Generalized Beam Theory (GBT) model is implemented which can effectively describe the failure mechanisms and is computationally efficient. GBT is a beam theory especially formulated for thin-walled sections with a capacity of determining the cross-sectional deformation through a linear combination of a set of pre-determined cross-sectional deformation modes. Here, to demonstrate the application and potential of GBT, a sample pipeline system is analyzed and the results are presented.

Keywords: Generalized Beam Theory, Trans-Alaska Pipeline System, Denali Earthquake

1. Introduction

The relative movement of the pipeline supporting system and the pipeline due to fault formation during an earthquake can cause large strain developments. Possible

failure mechanisms for pipelines in such case can be tensile fracture, cross-sectional ovalization, and buckling [1].

Pipelines and their interaction to the support system can be numerically simulated to the desired level of detail and accuracy using full scale, hybrid or simplified element formulations within finite element method (FEM). Full scale models with a combination of solid and shell elements [2] and hybrid models with combination of shell and beam elements [3] can adequately describe the respective failure mechanisms but they are computational expensive especially if a long section of the pipeline needs to be considered. On the other hand, simplified models with combination of beam and spring elements [4] are computationally inexpensive and capable of calculating the longitudinal deformation. However, they cannot describe cross-section response of a pipeline.

Here, to overcome these disadvantages a Generalized Beam Theory (GBT) is proposed which is fundamentally a beam element coupled with a cross-sectional analysis using a combination of a set of predetermined cross-section deformation modes. GBT was originally developed by Schardt [5] and his co-workers at the Technical University of Darmstadt to handle open and closed thin-walled sections. Since then, several research were conducted with respect to circular pipe sections, such as exact element formulation in GBT using hyperbolic shape functions [6], warping and distortion transmission in coupled shell-GBT formulation [7] and development of axisymmetric and torsion deformation modes to partially overcome null transverse extension and membrane shear strain assumptions [8].

In this paper, the deformation of Trans-Alaska Pipeline System (TAPS) [9] due to 2002 Denali earthquake at Denali fault crossing is modeled using GBT to show the applicability of the method and evaluate possible damage of the pipeline caused by cross-sectional ovalization.

2. Linear formulation of GBT

In GBT the displacements (u, v, w) in local coordinate system (x, y, z) (figure1) are expressed in equation (1) based on the principle of separation of variables, which contains the superposition of orthogonal modal cross-section displacement functions for the longitudinal ${}^{k}u(\theta)$, tangential ${}^{k}v(\theta)$, and transverse perpendicular ${}^{k}w(\theta)$ directions expressed as a function of the polar coordinate θ and an amplification function ${}^{k}V(x)$ for each displacement functions k along the beam length. The subscript index after a comma indicates the derivative of the respective function, for example ${}^{k}V_{,x}(x)$ is the first derivative of the amplification function ${}^{k}V(x)$ in x.

$$u(x,\theta)=\sum_{k=1}^{\infty}{}^{k}u(\theta)\,{}^{k}V_{,x}(x),\quad v(x,\theta)=\sum_{k=1}^{\infty}{}^{k}v(\theta)\,{}^{k}V(x),\quad w(x,\theta)=\sum_{k=1}^{\infty}{}^{k}w(\theta)\,{}^{k}V(x) \tag{1}$$

For thin-walled Circular Hollow Section (CHS) the cross-sectional deformation can be exactly described by the linear combination of k number of shell-type deformation modes defined by two independent sets of orthogonal trigonometric functions.

$$ {}^{k}u(\theta) = \begin{cases} -r\,cos(m\theta) & \text{if } m = (k-1)/2 \text{ for } k = 1,3,5... \\ r\,sin(m\theta) & \text{if } m = k/2 \text{ for } k = 2,4,6... \end{cases} \tag{2} $$

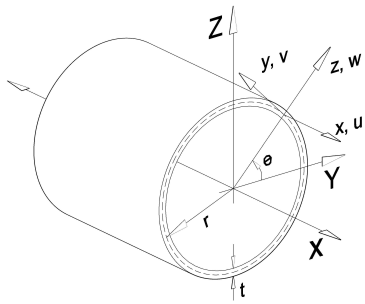

Figure 1: Thin-walled circular cross-section with global (X, Y, Z) and local ($\mathbf{x} \in [-\mathbf{L}/2, \mathbf{L}/2]$, $\mathbf{y} \in [\mathbf{0}, \mathbf{2\pi}]$, $\mathbf{z} \in [-\mathbf{t}/2, \mathbf{t}/2]$) coordinate systems.

The CHS beam member is defined in GBT with a complete plate behavior which satisfy the Love-Kirchhoff assumption and membrane behavior with Vlasov beam theory assumption of null transverse elongation and shear strain. The linear strain-displacement relationships [10] are given on equation (3) to (5) as a summation of membrane and plate strains. The relationship between the displacements u, v and w can be derived from the assumptions (i) null membrane in plane shear strain: $v_{,x} = -u_{,\theta}/r$ from first part of equation (5) and (ii) null membrane transverse strain: $w = -v_{,\theta} = u_{,\theta\theta}/r$ from first part of equation (4).

$$ \varepsilon_{xx} = u_{,x} - z w_{,xx} \tag{3} $$

$$ \varepsilon_{\theta\theta} = \frac{v_{,\theta} + w}{r} - z\left(\frac{w_{,\theta\theta} - v_{,\theta}}{r^2}\right) \tag{4} $$

$$ \varepsilon_{x\theta} = \frac{u_{,\theta}}{r} + v_{,x} - z\left(\frac{4r w_{,\theta x} - 3r v_{,x} + u_{,\theta}}{2r^2}\right) \tag{5} $$

2.1. Principle of virtual works

The GBT fundamental equilibrium equations are derived by means of the principle of the virtual work. The total potential energy of the member is defined by the virtual work due to the internal forces and the external loads. The equilibrium condition is defined if the total potential energy is zero. This gives:

$$ \delta\Pi = \delta U_{int} + \delta U_{ext} = 0 \tag{6} $$

The variation in the virtual work due to internal forces is defined as stress times a virtual strain component integrated over volume:

$$\delta U_{int} = \int_V (\sigma_{xx}\delta\varepsilon_{xx} + \sigma_{\theta\theta}\delta\varepsilon_{\theta\theta} + \tau_{x\theta}\delta\varepsilon_{x\theta})\mathrm{d}V \tag{7}$$

The constitutive relation between stresses and strains for isotropic elastic material in terms of the Young's modulus E, the shear modulus G and the Poisson's ratio μ are expressed by:

$$\sigma_{xx} = \frac{E}{1-\mu^2}(\varepsilon_{xx} + \mu\varepsilon_{\theta\theta}), \quad \sigma_{\theta\theta} = \frac{E}{1-\mu^2}(\varepsilon_{\theta\theta} + \mu\varepsilon_{xx}), \quad \tau_{x\theta} = G\varepsilon_{x\theta} \tag{8}$$

Substituting the GBT displacement functions on equation (1), the linear strain-displacement kinematic relation on equation (3-5) and constitutive relation on equation (17) into equation (7) and integrating it over the wall thickness the δU_{int} can be expressed as:

$$\begin{aligned}
\delta U_{int} = \sum_{k=1}^{\infty}\sum_{i=1}^{\infty}\int_{\frac{-L}{2}}^{\frac{+L}{2}}\oint\Bigg[&\frac{Et}{1-\mu^2}{}^{i}u(\theta)^{k}u(\theta)^{i}V_{,xx}(x)^{k}V_{,xx}(x)+\\
&\frac{\mu Et}{1-\mu^2}\Big(\frac{{}^{i}v_{,\theta}(\theta)+{}^{i}w(\theta)}{r}\Big)^{k}u(\theta)^{i}V(x)^{k}V_{,xx}(x)+\\
&\frac{Et^3}{12(1-\mu^2)}{}^{i}w(\theta)^{k}w(\theta)^{i}V_{,xx}(x)^{k}V_{,xx}(x)+\\
&\frac{\mu Et^3}{12(1-\mu^2)}\Big(\frac{{}^{i}w_{,\theta\theta}(\theta)-{}^{i}v_{,\theta}(\theta)}{r^2}\Big)^{k}w(\theta)^{i}V(x)^{k}V_{,xx}(x)+\\
&\frac{\mu Et}{1-\mu^2}{}^{i}u(\theta)\Big(\frac{{}^{k}v_{,\theta}(\theta)+{}^{k}w(\theta)}{r}\Big)^{i}V_{,xx}(x)^{k}V(x)+\\
&\frac{Et}{1-\mu^2}\Big(\frac{{}^{i}v_{,\theta}(\theta)+{}^{i}w(\theta)}{r}\Big)\Big(\frac{{}^{k}v_{,\theta}(\theta)+{}^{k}w(\theta)}{r}\Big)^{i}V(x)^{k}V(x)+\\
&\frac{\mu Et^3}{12(1-\mu^2)}{}^{i}w(\theta)\Big(\frac{{}^{k}w_{,\theta\theta}(\theta)-{}^{k}v_{,\theta}(\theta)}{r^2}\Big)^{i}V_{,xx}(x)^{k}V(x)+\\
&\frac{Et^3}{12(1-\mu^2)}\Big(\frac{{}^{i}w_{,\theta\theta}(\theta)-{}^{i}v_{,\theta}(\theta)}{r^2}\Big)\Big(\frac{{}^{k}w_{,\theta\theta}(\theta)-{}^{k}v_{,\theta}(\theta)}{r^2}\Big)^{i}V(x)^{k}V(x)+\\
&Gt\Big(\frac{{}^{i}u_{,\theta}(\theta)}{r}+{}^{i}v(\theta)\Big)\Big(\frac{{}^{k}u_{,\theta}(\theta)}{r}+{}^{k}v(\theta)\Big)^{i}V_{,x}(x)^{k}V_{,x}(x)+\\
&\frac{Gt^3}{12}\Big(\frac{4r^{i}w_{,\theta}(\theta)-3r^{i}v(\theta)+{}^{i}u_{,\theta}(\theta)}{2r^2}\Big)\Big(\frac{4r^{k}w_{,\theta}(\theta)-3r^{k}v(\theta)+{}^{k}u_{,\theta}(\theta)}{2r^2}\Big)\\
&{}^{i}V_{,x}(x)^{k}V_{,x}(x)\Bigg]\,r\,d\theta\,dx
\end{aligned} \tag{9}$$

Separating the cross-sectional integration, Equation (9) can be rewritten as:

$$\delta U_{int} = \sum_{k=1}^{\infty}\sum_{i=1}^{\infty}\int_{\frac{-L}{2}}^{\frac{+L}{2}} \Big[{}^{ik}C\ {}^{i}V_{,xx}(x)\,{}^{k}V_{,xx}(x) + {}^{ik}B\ {}^{i}V(x)\,{}^{k}V(x) + {}^{ik}D\ {}^{i}V_{,x}(x)\,{}^{k}V_{,x}(x) + {}^{ik}D_{\mu}\ \left[{}^{i}V(x)\,{}^{k}V_{,xx}(x) + {}^{i}V_{,xx}(x)\,{}^{k}V(x)\right] \Big] dx \quad (10)$$

The section properties are then expressed as:

$${}^{ik}C = \oint Q^{i}u(\theta)\,{}^{k}u(\theta) + K^{i}w(\theta)\,{}^{k}w(\theta) r\,d\theta \quad (11)$$

$${}^{ik}B = \oint Q\Big(\frac{{}^{i}v_{,\theta}(\theta) + {}^{i}w(\theta)}{r}\Big)\Big(\frac{{}^{k}v_{,\theta}(\theta) + {}^{k}w(\theta)}{r}\Big) + K\Big(\frac{{}^{i}w_{,\theta\theta}(\theta) - {}^{i}v_{,\theta}(\theta)}{r^2}\Big)\Big(\frac{{}^{k}w_{,\theta\theta}(\theta) - {}^{k}v_{,\theta}(\theta)}{r^2}\Big) r\,d\theta \quad (12)$$

$${}^{ik}D = \oint Gt\Big(\frac{{}^{i}u_{,\theta}(\theta)}{r} + {}^{i}v(\theta)\Big)\Big(\frac{{}^{k}u_{,\theta}(\theta)}{r} + {}^{k}v(\theta)\Big) + \frac{Gt^3}{12}\Big(\frac{4r^{i}w_{,\theta}(\theta) - 3r^{i}v(\theta) + {}^{i}u_{,\theta}(\theta)}{2r^2}\Big)\Big(\frac{4r^{k}w_{,\theta}(\theta) - 3r^{k}v(\theta) + {}^{k}u_{,\theta}(\theta)}{2r^2}\Big) r\,d\theta \quad (13)$$

$${}^{ik}D_{\mu} = \oint \mu Q\Big(\frac{{}^{i}v_{,\theta}(\theta) + {}^{i}w(\theta)}{r}\Big)^{k}u(\theta) + \mu K\Big(\frac{{}^{i}w_{,\theta\theta}(\theta) - {}^{i}v_{,\theta}(\theta)}{r^2}\Big)^{k}w(\theta) r\,d\theta \quad (14)$$

$$K = \frac{Et^3}{12(1-\mu^2)} \quad (15)$$

$$Q = \frac{Et}{(1-\mu^2)} \quad (16)$$

Here in order to achieve the diagonalization of the stiffness matrix the integration of the two warping functions for mode i and k must be eliminated for $i \neq k$. This must be true not only for the warping function itself, but also its derivation until the fourth order. Hence, to satisfy this unique property the orthogonal warping function on equation (2) are chosen by Schardt [5].

$$\oint {}^{i}u(\theta)\,{}^{k}u(\theta) d\theta = 0 \quad for\ i \neq k \quad (17)$$

The section properties coefficient C, B and D represent the section warping, transverse bending and torsional stiffness respectively. The summary of the warping functions and the corresponding cross-section properties are listed in the tables 1 and 2.

2.2. The finite element formulation

In the longitudinal direction, member analysis is performed using beam finite element method. The shape functions used to approximate the modal amplification ${}^{k}V(x)$ are

Table 1: Summary of warping functions.

Mode k	Warping Functions		
	$u(\theta)$	$v(\theta)$	$w(\theta)$
t	0	r	0
a	0	0	1
1	1	0	0
2m	$rsin(m\theta)$	$-mcos(m\theta)$	$-m^2sin(m\theta)$
2m+1	$-rcos(m\theta)$	$-msin(m\theta)$	$m^2cos(m\theta)$

Table 2: Summary of section properties for classical GBT, axisymmetric and torsional modes.

Mode k	Section Properties			
	C	B	D	D_μ
t	0	0	$G\pi tr(2r^2+\frac{3}{8}t^2)$	0
a	$K2\pi r$	$Q\frac{2\pi}{r}$	0	0
1	$Q2\pi r$	0	0	0
2m	$Q\pi r^3+K\pi rm^4$	$K\frac{\pi m^4}{r^3}(m^2-1)^2$	$G\frac{\pi t^3m^2}{3r}(m^2-1)^2$	$\mu K\frac{\pi m^4}{r}(1-m^2)$
2m+1				

the four node Lagrange cubic polynomial for the axial extension mode $k=1$ and the classic Hermite cubic polynomials for the rest of shell-type modes. Hence, the displacement amplification function $V(x)$ can be defined as a product of the shape function in a term vector $\{T_x\}$ of x, a completeness coefficient matrix $[Sh]$ of the shape function and the nodal deformations $\{\vartheta\}$:

$$^kV(x) = \left\{^kT_x\right\}\left[^kSh\right]\left\{^k\vartheta\right\} \tag{18}$$

2.3. Numerical example

As an example a cantilever pipe section is used to compare a GBT and an equivalent shell element model solution. As shown in figure 2, a $10m$ cantilever cylindrical pipe section with a diameter of $1.0m$ and a wall thickness of $10mm$ is considered and a projected area load of $0.01N/mm^2$ applied to the half section of the pipe. The elastic material parameters used are Young's modulus $E=205,000N/mm^2$ and shear modulus $G=78,846.2N/mm^2$. Poisson effect is neglected in this example. The GBT model is discretized into 100 beam elements and considered 7 deformation modes which can be somehow interpreted as degrees of freedom (DOF). On the other hand,

the equivalent shell element model is developed using 3600 quadrilateral elements with 6 DOF per node. The model is developed in ANSYS using SHELL181 element formulation which is based on Reissner-Mindlin kinematic assumption and uses a linear interpolation function.

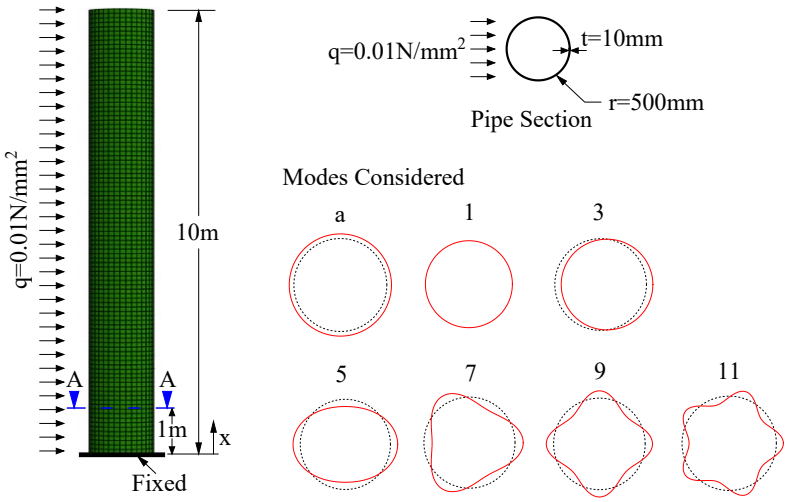

Figure 2: A cantilever cylindrical pipe example.

The first step in GBT is the transformation of the projected load q into the local coordinate system v and w direction. The load contribution in each mode is then determined by integration of the modal decomposition which is the inner product of the projected load with the deformation modes on equation (2). In this example, there is no participation from even modes since this integral is zero. Detailed linear GBT solution procedure can be found in [6]. In figures 3 and 4 the results of GBT is presented in comparison with shell element results. The displacements in figure 3 are the resultant displacement of Y, v and Z, w directions.

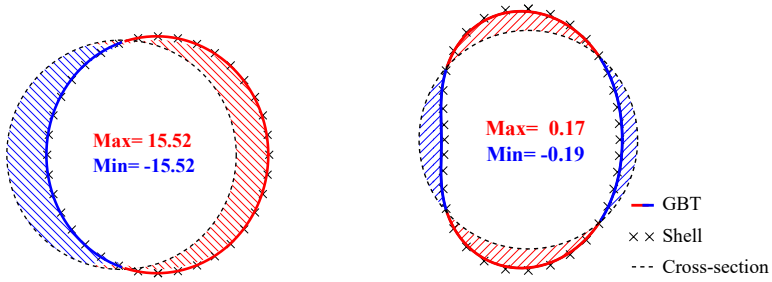

(a) Tip global displacement (scaled by 10)

(b) Local deformation at section A (scaled by 10^3)

Figure 3: Comparison of displacements in mm

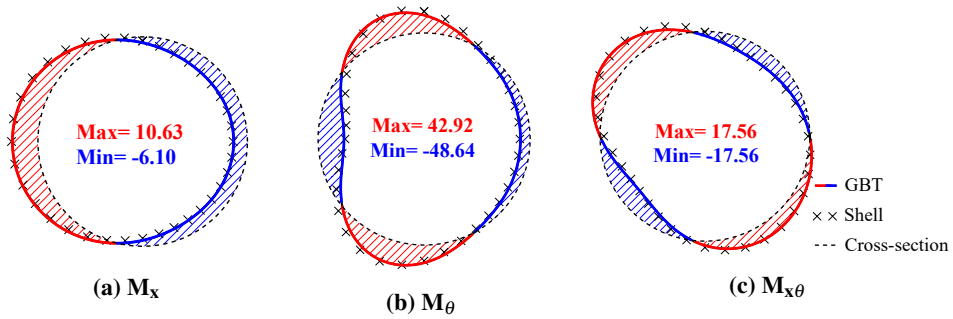

Figure 4: Comparison of bending moment at section A in Nmm/mm.

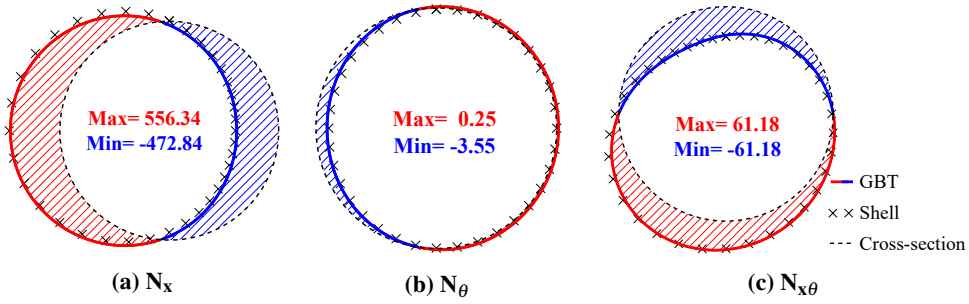

Figure 5: Comparison of normal force at section A in N/mm.

Table 3: Summary of comparison of GBT and shell results.

	M_x	M_θ	$M_{x\theta}$	N_x	N_θ	$N_{x\theta}$	U_{local}	U_{global}
Relative mean difference (%)	3.82	−8.72	1.02	6.18	−7.52	−4.72	−1.92	0.03
Standard deviation (%)	12.18	25.63	29.28	14.23	21.67	14.08	27.09	–

Table 3 shows the quantitative difference between the GBT and shell model using the mean of the relative difference of the curve plotting points and its standard deviation.

3. Trans-Alaska Pipeline System (TAPS)

TAPS is a 1287km long pipeline system with 1219mm diameter crossing Alaska from north to south transporting crude oil [9] [11]. The above ground part of the pipeline was designed as in a zigzag configuration with a sliding pipe support which allows the pipe to contract and expand due to temperature change and to resist seismic movements by sliding laterally and longitudinally. In order to limit these movements, the pipeline was anchored at certain distances using a high friction resistance support.

The part of TAPS which has been considered in this study is the 579m length pipeline section at the Denali fault crossing. This section of the pipeline was supported at approximately 18m intervals at the ground level on a crossbeam. The coefficients of

static and dynamic friction between the sliding pipe shoe and the beam support are 0.10 and 0.05 respectively (Figure 8a). These beams in the fault zone were arranged and sized according to the type of fault which in this case is a right lateral strike-slip fault (Figure 6). Anchors were located at north and south end of the special Denali fault crossing zone.

3.1. GBT model of TAPS

A GBT model has been developed for the length of the pipeline starting from the north end upto the south end anchor points including all the grade beam supports in the design fault zone and some vertical support members near the anchors. The 2002 Denali earthquake caused a right lateral horizontal slip of about 5.50m at the pipeline fault crossing putting the pipeline under compression. This fault displacement is introduced into the GBT model as a prescribed displacement at the supports based on the post earthquake measurements done on the positions of the pipe shoes and the beam supports (Figure 6). Here, the major advantage of the GBT model is the capacity to determine the extent of the pipe cross-section ovalization due to the excessive transverse bending caused by the fault displacement.

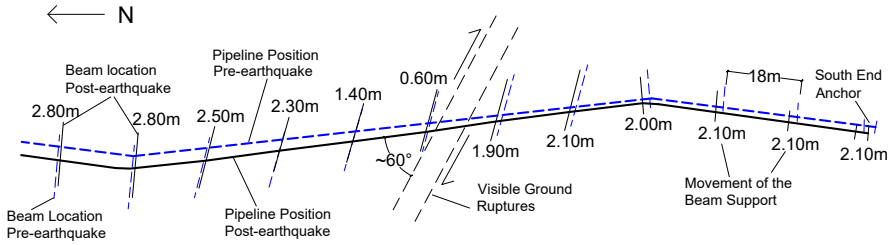

Figure 6: Schematic of the pipeline crossing of the Denali fault [9].

The GBT model in figure 7 is made up of 720 elements (1m element size) with four local modes (5, 7, 9 and 11) in addition to the global modes. In the model there are 41 supports in every 18m distance. The DOF in the vertical direction is not considered in

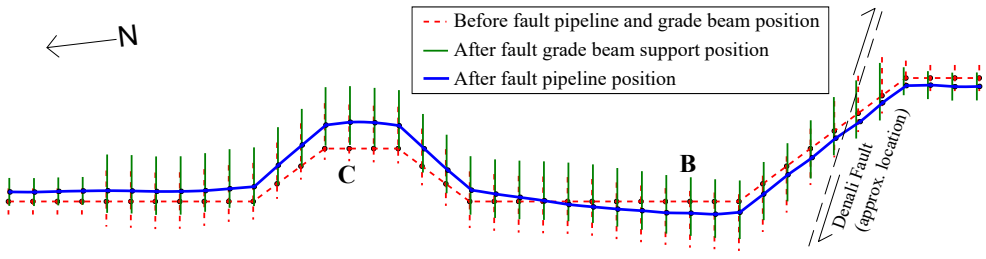

Figure 7: GBT model of the pipeline after introducing the fault displacements.

the model since the elevation profile of the pipeline was not available to the authors.

Hence, consideration of the vertical fault, which was additional to the major horizontal slip, was not possible. The GBT result of after fault position of the pipeline in figure 7 can be qualitatively compared with the actual fault displacement in figure 8b. In both cases bending or bowing of the pipeline and displacement of the pipe shoe to the outward direction is observed to accommodate the compressive displacement.

(a) Before fault slip **(b) After fault slip**

Figure 8: TAPS at the fault crossing [9].

Possible local damage of the pipeline caused by cross-sectional ovalization and large stress development can be identified at any section of the GBT model. Here, two sections (**B** and **C**) with large traversal displacement are selected as shown in figure 7.

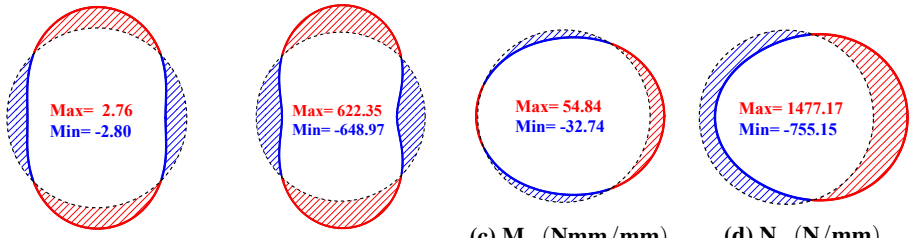

(a) U_{local} **(mm) (scale** 10^2**)** **(b)** M_θ **(Nmm/mm)** **(c)** M_x **(Nmm/mm)** **(d)** N_x **(N/mm)**

Figure 9: Section B local deformation (ovalization) and major section forces.

According to the GBT cross-sectional analysis at section **B** (Figure 9) and at section **C** (Figure 10) the maximum longitudinal axial stress are 126.25MPa and 308.68MPa respectively. The cross-sectional ovalization (Figure 9a and 10a) which is mainly caused by the transverse bending moment is well below the elastic deformation limit of the pipe in both sections .

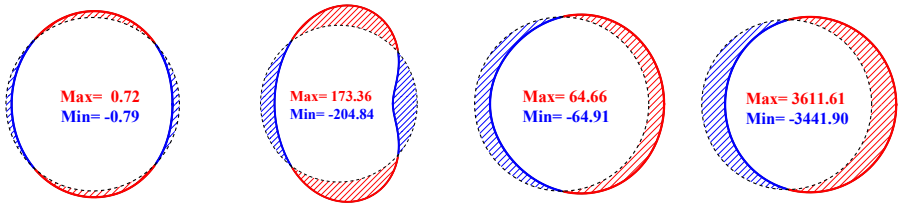

(a) U_{local}(mm) (scale 10^2) (b) M_θ (Nmm/mm) (c) M_x (Nmm/mm) (d) N_x (N/mm)

Figure 10: Section C local deformation (ovalization) and major section forces.

4. Conclusion

Using a numerical example and an actual case study the potential of GBT is demonstrated in this paper. After considering the several assumptions made in the TAPS model, the GBT results are quite satisfactory and comparable with the actual post-earthquake results. The incredible computational speed of GBT in comparison with an equivalent shell model, makes it suitable for long pipeline analyses.

Currently studies are being conducted to improve the boundary conditions, to consider the dynamic effect and extending the linear GBT formulation into nonlinear analyses to include the coupling effect of the deformation modes.

5. Acknowledgment

The authors gratefully acknowledge the support from the Horizon 2020 Programme of the European Commission under the MSCA-RISE-2015-691213-EXCHANGE-Risk grant (Experimental and Computational Hybrid Assessment of NG Pipelines Exposed to Seismic Risk, www.exchange-risk.eu).

References

[1] N. K. Psyrras, A. G. Sextos, Safety of buried steel natural gas pipelines under earthquake-induced ground shaking: a review, Soil Dynamics and Earthquake Engineering 106 (2018) 254–277.

[2] P. Vazouras, S. A. Karamanos, P. Dakoulas, Finite element analysis of buried steel pipelines under strike-slip fault displacements, Soil Dynamics and Earthquake Engineering 30 (11) (2010) 1361–1376.

[3] D. H. Lee, B. H. Kim, H. Lee, J. S. Kong, Seismic behavior of a buried gas pipeline under earthquake excitations, Engineering structures 31 (5) (2009) 1011–1023.

[4] L.-L. Wang, K.-M. Cheng, Seismic response behavior of buried pipelines, Journal of Pressure Vessel Technology 101 (1) (1979) 21–30.

[5] R. Schardt, Verallgemeinerte technische Biegetheorie: Lineare Probleme, Springer-Verlag, 2013.

[6] M. Bianco, C. Könke, A. Habtemariam, V. Zabel, Exact finite element formulation in generalized beam theory, International Journal of Advanced Structural Engineering 10 (3) (2018) 295–323.

[7] M. J. Bianco, A. K. Habtemariam, C. Könke, V. Zabel, Analysis of warping and distortion transmission in mixed shell–gbt (generalized beam theory) models, International Journal of Advanced Structural Engineering (2019) 1–18.

[8] N. Silvestre, Generalised beam theory to analyse the buckling behaviour of circular cylindrical shells and tubes, Thin-Walled Structures 45 (2) (2007) 185–198.

[9] D. G. Honegger, D. J. Nyman, E. R. Johnson, L. S. Cluff, S. P. Sorensen, Trans-alaska pipeline system performance in the 2002 denali fault, alaska, earthquake, Earthquake Spectra 20 (3) (2004) 707–738.

[10] J. L. Sanders Jr, Nonlinear theories for thin shells, Quarterly of Applied Mathematics 21 (1) (1963) 21–36.

[11] S. P. Sorensen, K. J. Meyer, Effect of the denali fault rupture on the trans-alaska pipeline, in: Advancing Mitigation Technologies and Disaster Response for Lifeline Systems, 2003, pp. 547–555.